HIGH-Q, LOW IMPEDANCE POLYSILICON RESONATORS WITH 10 NM AIR GAPS

Tiffany J. Cheng and Sunil A. Bhave
Cornell University, Ithaca, NY, USA

ABSTRACT

This paper presents a fabrication process to manufacture air-gap capacitively-transduced RF MEMS resonators. 2-port measurements show motional impedance (R_x) < 1.3kΩ and quality factor (Q) > 65,000 at 223MHz in vacuum. The fabrication process involves depositing a dual-layer spacer of 10nm of SiO_2 and 90nm of hafnia via atomic layer deposition (ALD) followed by oxide release. Nanometer air gaps are achieved, while the hafnia provides reliability against shorting of resonator and electrode. Consistent performance was achieved across multiple devices, demonstrating the robustness of the process.

INTRODUCTION

With exceptionally high quality factors, low power consumption, and CMOS compatibility, MEMS resonators provide an attractive solution to realizing fully integrated RF systems. It has recently been demonstrated that bulk resonators driven by internal dielectric transduction can achieve Q > 4,000 at 6.2GHz [1]. While the motional impedances of these devices scale favorably with frequency, the R_x versus frequency trend reported in [1] indicates impedances in excess of 200kΩ for frequencies below 1GHz. This impedance is prohibitively large for lower frequency applications, such as local oscillators used in telecommunications, which operate in the 1MHz to 1GHz frequency range. For sub-GHz applications, other methods of reducing motional impedance are necessary.

Piezoelectric resonators have achieved motional impedances as low as 24Ω at UHF, but the inherent loss of piezoelectrics limits the Q of the device to a few thousand [2]. Capacitively-driven resonators typically have much higher impedances that are on the order of a few kΩ [3][4][8]. However, capacitively-transduced silicon resonators have consistently achieved the highest Qs among MEMS resonators in the sub-GHz range. Furthermore, fabrication of these resonators involves CMOS compatible materials and micromachining techniques that can be easily integrated into batch IC processes.

Several groups have experimented with increasing the electromechanical coupling factor η_e of capacitively driven air gap resonators by optimizing one or more of the parameters that determine η_e: transduction area, polarization voltage, and gap spacing g. Thick SiBARs with $600\mu m^2$ transduction areas have achieved an R_x of 680Ω at 85.9MHz with a Q of 22,400 in SOI [3]. There has been interest in reducing the gap in order to capitalize on the inverse relation between R_x and g^4. However, reliable fabrication of resonators transduced with thin air-gap capacitors is difficult not only because of fabrication limitations, but also because of increased risk of shorting.

Shorting can be prevented by inserting a dielectric between the resonator and electrode. Previously, devices have been made in which a high-κ dielectric was deposited into the gap of an already released structure [5][6], achieving 32nm air-gaps. However, those resonators exhibited a Q drop of >10× after hafnia coating due to losses introduced by the dielectric film on the resonator.

In contrast to the additive method of [5][6], our process utilizes a sacrificial spacer to create the air-gap, and is therefore not restricted by the starting gap of a released resonator. Hafnia is deposited only on the electrode side of the capacitive transducers, maintaining a pristine silicon resonator without any mass-loading or Q degradation. Furthermore, the process does not require an extra mask and lithography step to etch the dielectric from the bond-pads. Using this method, we fabricated resonators with transduction gaps consisting of 90nm hafnia and 10nm air, achieving R_x < 1.3kΩ and Q > 65,000 at VHF.

THEORY

Fig.1 shows the cross-section of a bar resonator driven by a capacitor composed of a dielectric layer and an air gap with permittivities of $\kappa\epsilon_0$ and ϵ_0, respectively. If $C_2 >> C_1$, the effective capacitance is

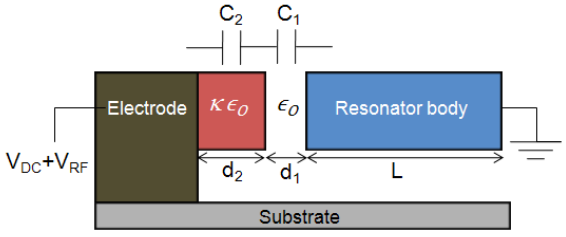

Figure 1. *Cross-sectional view of a bar resonator actuated through a dual-layer capacitor. ϵ_0 is the permittivity of free space. V_{DC} and V_{RF} are bias and RF input voltages, respectively.*

978-1-4244-5763-2/10/$26.00 ©2010 IEEE

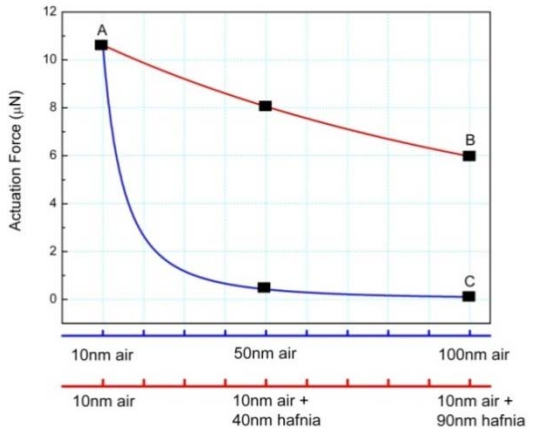

Figure 2. *Sinusoidal actuation force vs. gap thickness for a hafnia+air gap resonator and an air-gap resonator. The calculation assumes 15V DC, 100mV RF, and transduction area of 80μm^2.*

roughly that of the air gap [5]. However, the C_1 of our devices is comparable to C_2 because the air gap is much narrower than the hafnia thickness, resulting in an appreciable voltage drop across the hafnia. In our case, the 90nm hafnia (κ=27) layer drops 1/4 of the input voltage, meaning that the total capacitance is actually 3/4 of the 10nm air gap capacitance. Fig.2 assesses the reduction in capacitive driving force with increasing hafnia thickness, assuming an air gap of 10nm. For comparison, the actuation force of a conventional air-gap transduced resonator is also shown. Starting from equal forces (point A), the force drop of the hafnia+air-gap resonator is much less dramatic compared to that of the air-gap device. Increasing the hafnia thickness to 90nm (point B) is far more favorable than increasing the air gap by the same amount (point C).

Eqns. (1)-(5) give ${\eta_e}^2$ and the equivalent circuit model for the resonator of Fig.1 driven in bulk longitudinal mode at its resonant frequency $f = \frac{n}{2L}\sqrt{\frac{Y}{\rho}}$. A is the capacitor transduction area, n is the mode number, and Y and ρ are the Young's modulus and density of polysilicon, respectively.

$$ {\eta_e}^2 = \frac{A^2 {V_{DC}}^2 {\epsilon_0}^2 \kappa^4}{(d_2 + d_1\kappa)^4} \quad (1) $$

$$ R_x = \frac{n\pi(d_2 + d_1\kappa)^4\sqrt{Y\rho}}{2AQ{V_{DC}}^2{\epsilon_0}^2\kappa^4} \quad (2) $$

$$ C_x = \frac{2AL{V_{DC}}^2{\epsilon_0}^2\kappa^4}{n^2\pi^2 Y(d_2 + d_1\kappa)^4} \quad (3) $$

$$ L_x = \frac{L(d_2 + d_1\kappa)^4\rho}{2A{V_{DC}}^2{\epsilon_0}^2\kappa^4} \quad (4) $$

$$ C_0 = \frac{C_1 C_2}{C_1 + C_2} \quad (5) $$

FABRICATION

Fundamental mode bar resonators (Fig.3) were fabricated using the process in Figs. 4-5. Vertical polysilicon stubs placed at the displacement nodes anchor the body and bias the resonator. To create the dual layer capacitor, 10nm of SiO_2 and 90nm of hafnia were deposited in immediate succession in an Oxford ALD system. Fig.7 is an SEM of a resonator fabricated in this process of length 18μm, width 40μm, and thickness 2 μm. An effective air gap of 10nm $\pm$ 2nm was calculated from impedance measurements (Agilent 4287 LCR meter) of 14 devices. Fig.8a shows the transmission response of this device. For comparison to typical air-gap resonators and assessment of Q degradation, we then etch the hafnia (Fig.6), opening a 100nm air-gap, and re-measure the same resonator (Fig.8b).

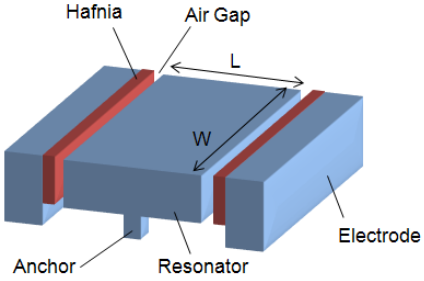

Figure 3. *Capacitively-transduced bar resonator with vertical anchors.*

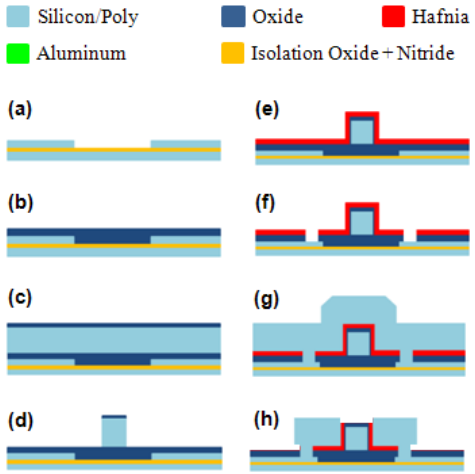

Figure 4. *(a) Deposit and pattern poly-Si routing layer (b) Deposit sacrificial oxide (c) Deposit and pattern poly-Si and SiO_2 hard mask for dry etch (d) Dry etch poly-Si to define resonator body (e) ALD 10nm SiO_2 followed by 90nm of HfO_2 (f) Define anchors (g) Deposit poly-Si for electrodes (h) CMP and remove hafnia for metallization*

Figure 5. *After Fig. 4h and metallization, hafnia + air gap devices are vapor HF released to achieve 10nm air gap.*

Figure 6. *An additional wet etch to remove hafnia after the step in Fig. 5 resulted in 100nm air gap devices.*

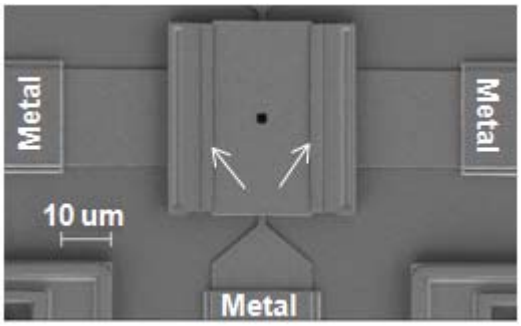

Figure 7. *SEM of a 222MHz resonator. Arrows indicate the 10nm air + 90nm hafnia gap. The gap was too small to be adequately imaged in SEM.*

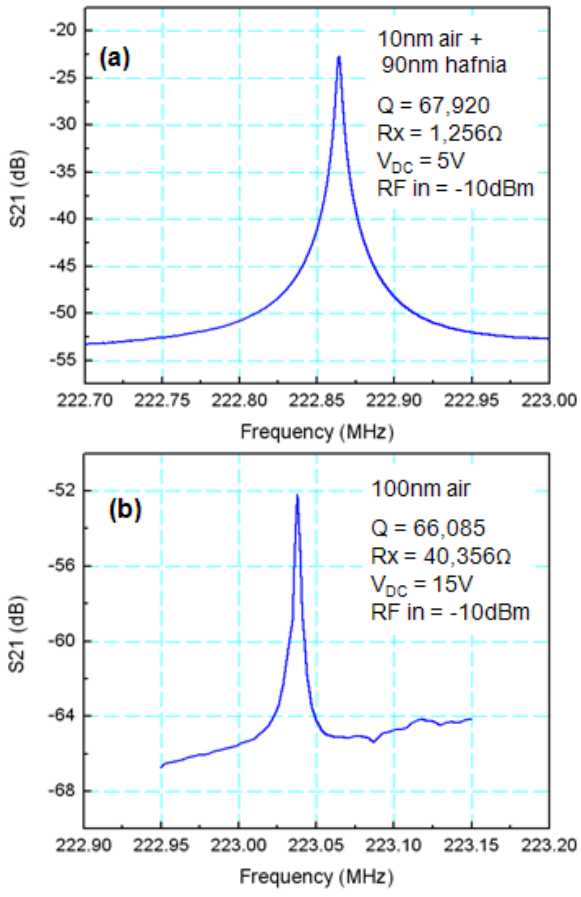

Figure 8. *The same resonator is actuated through a 10nm air + 90nm hafnia gap (a) and a 100nm air gap (b).*

RESULTS AND DISCUSSION

Standard 2-port measurements using an Agilent 8364B network analyzer were performed on all devices in vacuum. R_x was extracted from S_{21} according to (6).

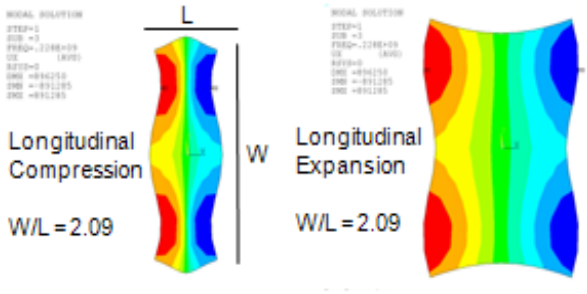

Figure 9. *Ansys simulation of the fundamental mode of a 18µm x 40µm x 2µm resonator shows distortion of the bar edges, which causes motional charge cancellation.*

$$10^{S_{21,dB}/10} = \frac{(2Z_0)^2}{(2Z_0 + R_x)^2} \quad (6)$$

Comparison of device performance before and after hafnia removal (Fig.6) shows that the device retained the original Q, while the R_x increased by 32×. This confirms that the 10nm sacrificial oxide spacer was cleanly removed without any residual mass-loading or damping effect on the resonator.

From (2), we expect a motional impedance of 90Ω for the device in Fig.8a, which is far off from the measured $R_x$of 1,256Ω. The predicted R_x for the 100nm air gap device is 33.6kΩ. The discrepancy for the 100nm air gap device could easily be due to process variation – assuming a gap of 105nm gives a predicted R_x of 40.8kΩ. The series resistance should be very low because of metal routing, and therefore is an unlikely cause for the inconsistency between theoretical and measured impedances for the hafnia+air gap device. Ansys simulations of the device in Fig.8a show that there is significant mode distortion of the bar edges (Fig.9). There is a strong possibility that the large W/L aspect ratio of the resonators has caused mode-shape distortion, which can lead to charge cancellation and reduction in the electromechanical coupling efficiency [7]. Initial simulations suggest that mode distortion is force dependent, which would explain why the 100nm air gap resonator performs as predicted, while the hafnia+air gap device does not. Future work will assess the impact of large W/L ratios on the transduction efficiency of these devices.

Fourteen resonators selected from random locations on an 8-inch wafer display an extremely tight $f{\cdot}Q$ scatter matrix, demonstrating reliable manufacturability of these devices (Fig.10). The process is also scalable to higher frequencies - Fig.11 demonstrates a 523.3MHz resonator with Q of 19,563 and R_x of 3.82kΩ. Table 1 summarizes the performance of our devices and that of 4 other low-impedance VHF resonators driven through air-gap capacitors. Our resonators compare very favorably in terms of both R_x and $f{\cdot}Q$.

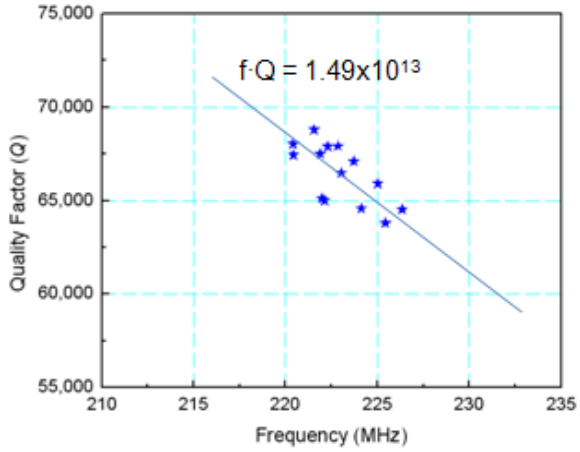

Figure 10. *The scatter data is of 14 devices from various dies on an 8-in. wafer. The data points tightly fit around f·Q = 1.49×10[13].*

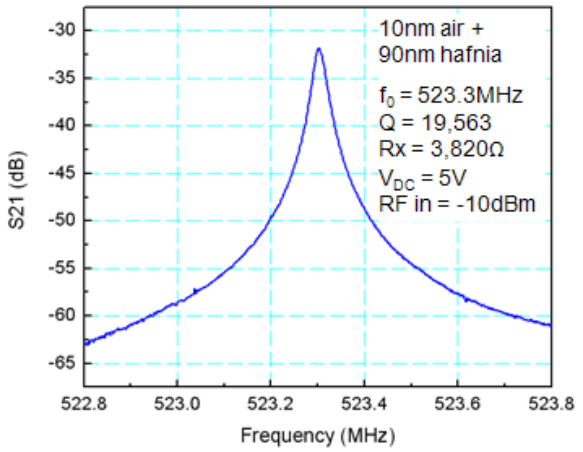

Figure 11. *2-port capacitive measurement of a 523.3MHz resonator.*

CONCLUSION

We present a fabrication process that enables the manufacture of 10nm transduction gaps, while maintaining the intrinsic Q of the resonator. This is done by dual ALD deposition of 90nm hafnia and 10nm sacrificial SiO_2, which leaves hafnia only on the electrode. Our analysis shows that most of the voltage is dropped across the narrow air gap, resulting in large actuation forces and low R_x on the order of 1kΩ. In conclusion, our process provides a streamlined, reliable way of achieving high electromechanical coupling in capacitively-transduced high-Q silicon resonators targeting sub-GHz applications.

ACKNOWLEDGEMENTS

This work was funded by the National Science Foundation Graduate Research Supplement grant. The authors would like to thank the RF MEMS group at Sony Corporation.

Table 1. *Performance comparison of our device with four other capacitively transduced air-gap resonators (preference given to low-impedance).*

Reference	Material	Rx (loaded) [Ω]	Frequency [MHz]	*Q*	*f·Q*
[3]	SCS	680	85.9	22,400	1.9×10^{12}
[4]	Poly-Si	11,300	61	161,000	9.8×10^{12}
[8]	SCS	10,000	5	103,000	5.7×10^{11}
[5]	Poly-Si	685	59.3	7,368	4.4×10^{11}
This Paper	Poly-Si	1,256	222.8	67,920	1.5×10^{13}

REFERENCES

[1] D. Weinstein, et al, "Frequency Scaling and Transducer Efficiency in Internal Dielectric Transduced Silicon Bar Resonators" Transducers'09, Denver, CO, June 21-25, 2009, pp. 708-711.

[2] G.Piazza, et al, "One and Two Port Piezoelectric Higher Order Contour-Mode MEMS Resonators for Mechanical Signal Processing", *Solid-State Electronics,* vol. 51, pp. 1596–1608, 2007.

[3] S. Pourkamali, "Low-Impedance VHF and UHF Capacitive Silicon Bulk Acoustic Wave Resonators - Part II: Measurement and Characterization," IEEE Transactions on Electron Devices, vol. 54, no. 8, pp. 2024-2030, 2007.

[4] Y.-W. Lin, et al, "Low Phase Noise Array-Composite Micromechanical Wine-Glass Disk Oscillator," IEEE International Electron Devices Meeting, Washington, DC, DC.5-7, 2005, pp.287-290.

[5] L.-W. Hung, et al, "Capacitive Transducer Strengthening Via ALD-Enabled Partial-Gap Filling" Hilton Head, SC, June 1-5, 2008, pp.208-211.

[6] M. Akgul, et al, "Oscillator Far-From-Carrier Phase Noise Reduction Via Nano-Scale Gap Tuning of Micromechanical Resonators" Transducers'09, Denver, CO, June 21-25, 2009, pp. 798-801.

[7] Siavash Pourkamali, Ph.D Thesis, December 2006, Georgia Institute of Technology.

[8] K. Sundaresan, et al, "Electronically Temperature Compensated Silicon Bulk Acoustic Resonator Reference Oscillators" IEEE Journal of Solid-State Circuits, vol.42, no.6, pp.1425-1434, 2007.